Journal of The Electrochemical Society, **150** (2) A143-A148 (2003)
0013-4651/2002/150(2)/A143/6/$7.00 © The Electrochemical Society, Inc.

Criteria for Reliable Electrochemical Impedance Measurements on Li-Ion Battery Anodes

Chunsheng Wang,[a,*,z] A. John Appleby,[a,*] and Frank E. Little[b]

[a]*Center for Electrochemical Systems and Hydrogen Research, and* [b]*Center for Space Power, Texas Engineering Experiment Station, Texas A&M University, College Station, Texas 77843, USA*

Specially designed five-electrode cells contained two types of mixed ionic-electronic conductor (MIEC) lithium-insertion anodes. These were graphite or $Sn_{1.3}Al_{0.3}Ti_{1.7}O_{1.95}(PO_4)_3$ tin composite oxide (TCO) bonded powders sandwiched between nickel mesh current collectors as working lithium-ion anodes, with Li foils on both sides as reference electrodes, outside of which were two further Li foils, or a Li foil and an electrode identical to the graphite anode, as counter electrodes. The cells were used to investigate the influence of the counter and reference electrodes on the impedance of the working electrode. The impedance of the graphite anode measured using a Li foil counter electrode was higher than that using the graphite counter electrode. This was because the low electrochemical reaction kinetic rate on the Li counter electrode influenced the electric field and potential distribution in the intervening electrolyte, resulting in an unstable reference electrode potential. Using the only one Li foil as the counter electrode with the reference electrode on the opposite side can reduce the influence of the counter electrode(s) on its impedance. The transmissive impedance and ionic impedances of both types of MIEC anodes were also studied.
 [DOI: 10.1149/1.1530150]

Manuscript submitted June 4, 2002; revised manuscript received July 17, 2002. Available electronically December 23, 2002.

Electrochemical impedance spectroscopy (EIS) is a more powerful technique for lithium-ion electrode kinetic analysis than microperturbation methods such as small amplitude cyclic voltammetry, potential intermittent titration (PIT), and galvanostatic intermittent titration (GIT). This is because it can give the individual impedance for each reaction process, including that of the electrolyte, the passivation layer, charge-transfer, and Li diffusion, provided that the individual time constants are separable. Conventional three-electrode electrochemical cells with metallic Li reference and counter electrodes are most frequently used for such measurements. In three-electrode EIS, the potentiostat applies and measures potentials between the working electrode (WE) and the reference electrode (RE), and the counter electrode (CE) serves to collect the induced current. The WE impedance should therefore be independent of CE behavior. In practice, the Li counter electrode[1] and the shape and position of the RE[2] may have a significant influence on the impedance of the WE in the three-electrode configuration. This is because the usual way of protecting a RE from local potential distributions, *i.e.*, via a Luggin capillary, is not generally used in such cells due to constructional difficulties. Ong and Yang[1] found that the impedance of graphite WE measured with an identical graphite CE is more reliable than that measured with a Li foil CE. They believed that after several charge-discharge cycles, the surface of the Li counter electrode is severely modified by the formation of a solid electrolyte interphase (SEI) film, which influences the WE current.[1] If this is so, then the SEI film formed on graphite electrode identical with the working anode, and used as a counter electrode in the two-electrode configuration, should also influence the graphite anode EIS.

To verify this influence, two special five-electrode cells were constructed. These had $C_2(Li)$-$R_2(Li)$-$G_{1,2}$-$R_1(Li)$-$C_1(Li)$ and $C_2(Li)$-$R_2(Li)$-$G_{1,2}$-$R_1(Li)$-$C1(G_3)$ configuration, in which two lithium foils [$C_2(Li)$, $C_1(Li)$] or one lithium and one graphite electrode identical to the WE [$C_2(Li)$, $C_1(G_3)$] were external parallel CEs, and the inner two lithium foils were REs. In another cell, the tin composite oxide (TCO) of composition $Sn_{1.3}Al_{0.3}Ti_{1.7}O_{1.95}(PO_4)_3$ was used as the WE. The impedances of graphite and TCO electrodes were compared by using different CE and RE geometries.

Experimental

Electrode and cell preparation.—Johnson-Matthey JM 287 graphite powder (particle diam *ca.* 15 μm, Brunauer-Emmett-Teller (BET) area 13.5 $m^2\ g^{-1}$) and the glass $Sn_{1.3}Al_{0.3}Ti_{1.7}O_{1.95}(PO_4)_3$ were used as intercalation anode materials. The latter was selected because of the high ionic conductivity of $Li_{1.3}Al_{0.3}Ti_{1.7}(PO_4)_3$ ceramic (2×10^{-3} S cm^{-1}), which is formed after first discharge (Li insertion). The glass was prepared in a modification of the method used by Fu.[3] Lithium mixed phosphate glasses were prepared from appropriate mixed reagent-grade SnO_2, $Al(OH)_3$, TiO_2, and $NH_4H_2PO_4$ powders in an alumina crucible in an electric furnace. The batch was initially kept at 700°C for 1.0 h to release volatile products, then heated to 1500°C for 2.0 h. The melt was poured onto a stainless steel plate and pressed with a second plate. This was followed by heat-treatment at 960°C for 6.0 h. Composite graphite and TCO powder electrodes were sandwiched between two nickel screen current collectors and were prepared as in previous work from a mixture of 85 wt % active material (*ca.* 50 mg) with 7 wt % carbon black and 8 wt % poly(vinylidene fluoride) (PVDF) binder in 1-methyl-2-pyrrolidinone solvent. After drying overnight at 110°C, the 2.0 cm^2 geometric area, 0.8 mm thick electrodes were pressed to the configuration shown previously.[4,5] To simulate the real conditions of a Li-ion cell, the Ni sandwiched $Sn_{1.3}Al_{0.3}Ti_{1.7}O_{1.95}(PO_4)_3$ electrode was wrapped in a Celgard 2400 separator and then compressed between two PTFE holders with small holes to allow penetration of electrolyte. Electrochemical measurements were conducted in the five-electrode PTFE cell shown in Fig. 1. The surface area of Li CE(s) was much larger than that of the Li RE(s). The graphite electrode used as a second CE was identical with the graphite WE. All potentials are given *vs.* the Li/Li^+ reference electrode in the electrolyte used, 1.0 M lithium hexafluorophosphate ($LiPF_6$) in a 4:1:3:2 by volume ethylene carbonate (EC)-propylene carbonate (PC)-dimethylcarbonate (DMC)-ethyl methyl carbonate (EMC) mixture (high-purity lithium battery grade, Mitsubishi Chemical Co.). Electrochemical cells were assembled in an argon-filled glove box. Discharge (lithium intercalation) and charge (lithium extraction) characteristics were measured between +0.0 and +1.5 V at constant current using an Arbin (College Station, TX) automatic battery cycler, and the voltage differences across both sides of $Sn_{1.3}Al_{0.3}Ti_{1.7}O_{1.95}(PO_4)_3$ electrode were used to monitor their relative conductivity change.

The graphite WE [connected to the identical G_3 CE together in $C_2(Li)$-$R_2(Li)$-$G_{1,2}$-$R_1(Li)$-$C_1(G_3)$ cell] was discharged/charged on both sides for four cycles at 25°C, then cycled four times at

* Electrochemical Society Active Member.
z E-mail: cswang@tamu.edu

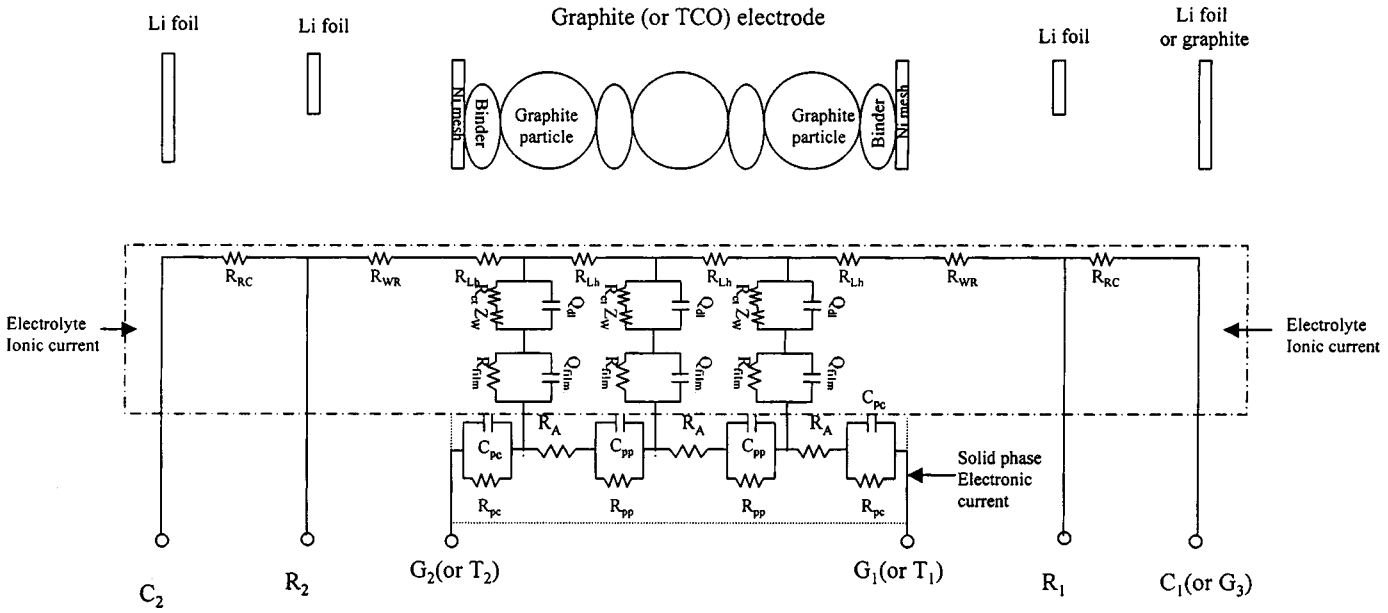

Figure 1. Schematic diagram of cell with porous ion graphite (or TCO) anode. The transmission line equivalent circuit for Li ion insertion/extraction into active electrode is also shown. R_A, R_{Lh}, R_{WR}, and R_{RC}: Electronic resistance of active particle, ionic electrolyte resistance in porosity, reference to WE ionic resistance, and reference to CE ionic resistance. R_{pc}, R_{pp}, R_{film}, and R_{ct}: Active particle-to-current collector, particle-to-particle, SEI film, and charge-transfer resistances. C_{pc} and C_{pp}: Particle-to-current collector and particle-to-particle contact capacitances. Q_{film} and Q_{dl}: Constant phase elements for the film and for the double layer. Z_W: Finite Warburg element for lithium in electrode. C_1, C_2, R_1, and R_2: Li foils used as CEs 1 and 2, and REs 1 and 2. G_3: Graphite electrode used as alternative counter electrode, identical to $G_{1,2}$ working electrode. G_1, G_2, T_1, and T_2: Sides 1 and 2 of graphite and TCO electrodes.

−30°C, four times at +60°C, and given a final cycle at 25°C. After 2.0 h of relaxation following the initial three discharge to 0.0 V at 25°C and after the sixth discharge to 0.0 V at −30°C, special EIS protocols were performed on the WE. The second and thirteenth discharge-charge cycles were performed using GIT.

EIS measurement.—In each case, this was taken over the 65 kHz to 0.01 Hz frequency range at a potentiostatic signal amplitude of 5 mV, using a Solartron FRA 1250 frequency response analyzer and a Solatron model 1286 electrochemical interface. Measurements were performed after electrodes were left on open circuit for 2.0 h for potential stabilization. For clarity, the electrode impedance is given as $Z_{W_iR_jC_k}$, where W_i, R_j, and C_k are the WE, the RE(s), and CE(s), respectively. Subscripts i, j, and k each may be 1, 2, and 1,2. For example, $G_{1,2}$ indicates that both sides of the graphite WE were connected together, and $C_{1,2}$ indicates that the two Li CEs were connected together, so $Z_{G_{12}R_1C_{12}}$ is the graphite anode impedance as measured by connecting its G_1 and G_2 sides together as the WE, with C_1 and C_2 connected together as the CE, and using R_1 as the RE. The graphite electrode, G_3, was always operated with both sides connected together. If it and the Li foil C_2 were connected together as CE with R_1 as RE, the impedance of the graphite anode $G_{1,2}$ is expressed as $Z_{G_{12}R_1(G_3C_2)}$. The impedance of the two-electrode cell with no reference electrode(s) is given as $Z_{W_iC_k}$, where W_i and C_k are the WE and CE. $Z_{G_{12}G_3}$ is the impedance when the graphite counter electrode was used, with both sides of the working anode connected.

Results and Discussion

The influence of the CE on the impedance of the WE.—To investigate the influence of the CE on the graphite anode EIS, the electrode configuration C_2(Li)-R_2(Li)-$G_{1,2}$-R_1(Li)-$C_1(G_3)$ was used for EIS measurement (Fig. 1). Unlike the cell used by Ong and Yang,[1] a small-area Li foil was inserted between two identical graphite working ($G_{1,2}$) and counter electrodes (G_3) as a reference electrode. The C_2(Li)-R_2(Li)-$G_{1,2}$-R_1(Li)-$C_1(G_3)$ cell may be considered to be two three-electrode cells, *i.e.*, $G_{1,2}$-R_1(Li)-$C_1(G_3)$ and $G_{1,2}$-R_2(Li)-C_2(Li) or as a four-electrode cell with graphite G_3 and Li foil C_2 as the counter electrode and another small Li foil (R_1 or R_2) as the reference electrode. Figure 2 shows the impedance of this cell measured after the third discharge to 0.0 V, followed by short circuiting (*i.e.*, connecting $G_{1,2}$, G_3, C_2) overnight. For the ($G_{1,2}$)-R_1(Li)-$C_1(G_3)$ cell, the impedances of the two graphite electrodes were superposable, which confirmed that these two graphite electrodes were indeed identical (Fig. 2a).

Moreover, the sum of the two half-cell impedances ($Z_{G_{1,2}R_1C_3} + Z_{G_3R_1G_{1,2}}$) was the same as the two-electrode ($Z_{G_{1,2}G_3}$) impedance measurement, which confirmed that the EIS measurement was reliable. Similarly, in the $G_{1,2}$-R_2(Li)-C_2(Li) cell, the sum impedance of graphite ($G_{1,2}$) and Li electrodes (C_2) with R_2 as the RE ($Z_{G_{1,2}R_2C_2} + Z_{C_2R_2G_{1,2}}$) was almost the same as the two-electrode impedance ($Z_{G_{1,2}C_2}$). An interesting fact was that the impedance of the WE ($G_{1,2}$) measured using a Li foil (C_2) counter electrode was much larger than that measured using the identical porous graphite (G_3) CE (Fig. 2c), even though the validity of impedance had been confirmed via the two three-electrode cells. A reasonable explanation for this difference is now given.

In impedance measurement of the WE in a three-electrode cell, the voltage signal is acquired from the potential difference between the WE and RE, while the current is applied between the CE and WE. When the overall electrochemical reaction kinetics of the counter electrode process is similar in rate to that of the WE, *i.e.*, the case of the identical porous graphite counter electrode, the potential difference with a 5 mV amplitude superposed sine wave between the WE and RE during EIS measurement is similar to that between the RE and CE. Therefore, the electric field and local potential of the RE located at the midpoint between the WE and CE remained stable during EIS measurement. However, when the overall electrochemical reaction kinetics of the CE are much less rapid than those of the WE, *i.e.*, the Li foil case shown in Fig. 2b, the potential difference

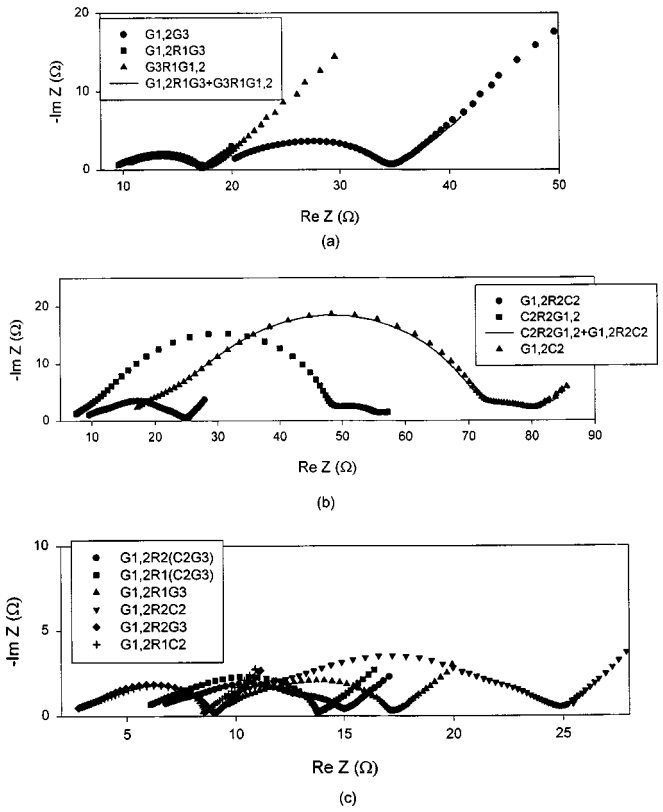

Figure 2. Impedances of electrodes in five-electrode cell with configuration C_2(Li)-R_2(Li)-$G_{1,2}$-R_1(Li)-C_1(G_3). EIS measured after short-circuiting (connecting $G_{1,2}$, G_3, C_2 together) overnight, following the third discharge to 0.0 V. Graphite counter electrode G_3 is identical with working anode $G_{1,2}$. The impedance of working electrode is given as $Z_{W_iR_jC_k}$, where W_i, R_j, and C_k are, respectively, the WE, the RE(s) and CE(s). Subscripts i, j, and k each may be 1, 2, and 1,2. $G_{1,2}$ indicates that both sides of the graphite WE were connected together. (C_2G_3) that C_2 is connected to G_3 as CEs. $Z_{W_iC_k}$ indicate a impedance of the two-electrode cell with no REs is given.

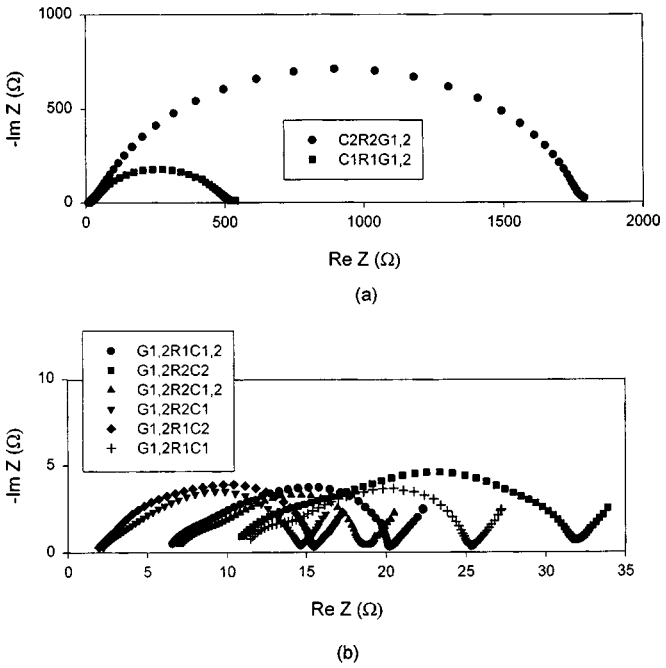

Figure 3. Impedances of two CEs (C_1 and C_2) and (b) graphite electrode ($G_{1,2}$) in five-electrode cell with configuration of C_2(Li)-R_2(Li)-$G_{1,2}$-R_1(Li)-C_1(Li). The EIS was measured after relaxation for 2.0 h after the third discharge to 0.0 V. $C_{1,2}$: Indicting C_1 and C_2 are connected together as CEs. $G_{1,2}$: As Fig. 2.

between the CE and RE is much greater than that between the WE and CE. Hence, the electric field distribution in the electrolyte between WE and CE changes during the measurement, in turn changing the local potential environment of the RE. The result is an overpotential change of the graphite WE, resulting in an apparently increased impedance. If this explanation is correct, measurement using both CEs G_3 and C_2 should decrease the impedance of the $G_{1,2}$ WE compared to the value measured using one Li CE (C_2), because a major part of the current passes through the less polarized G_3 CE. As expected, the diameter of the depressed semicircle measured using C_2 and G_3 together as the CE counter electrode is much smaller than that measured using a single Li foil alone, and is similar to that obtained using a single graphite CE, G_3 (Fig. 2c). This suggests that use of a graphite CE identical to the WE surfaces gives a more accurate impedance value. The reason for the smaller electrolyte resistance in the $G_{1,2}$ impedance measured using two CEs compared with that using a single CE is that the partial current flow between the second CE and the WE on the side opposite the RE reduces the effective electrolyte resistance.

To obtain reliable impedance data for graphite anodes in three-electrode cells, the overall electrochemical reaction kinetic rate at the CE should be at least equal or greater than that of the WE. That the impedance of a graphite electrode measured using a Li foil counter electrode was higher than that using an identical porous graphite counter electrode is due to the comparatively slow kinetics at the lithium CE which result from the large surface area of the porous graphite electrode. Therefore it is reasonable to believe that decreasing the surface area of Li counter electrode also causes an apparent increase in the impedance of the porous graphite electrode. To confirm this, the graphite CE was replaced by Li foil in a new five-electrode configuration C_2(Li)-R_2(Li)-$G_{1,2}$-R_1(Li)-C_1(Li). In this cell, the two Li counter electrodes had different surface areas. Figure 3 shows the impedances of the Li CEs and the graphite WE in this cell. The overall reaction rate at the high-area CE C_1 was much larger than that at C_2 (Fig. 3a). As expected, the impedance of the graphite WE $G_{1,2}$ measured using C_1 as the CE was smaller than that using C_2 (Fig. 3b), confirming the hypothesis. Similarly, measurements made using both Li foils (C_1 and C_2) further decreased the WE impedance (Fig. 3b).

The influence of the RE on the EIS of the WE.—A large potential change in the CE during EIS measurement influences the electric field and potential distributions in the electrolyte between the WE and CE(s) and results in fluctuating Li RE potentials for unprotected REs. However, the potential change in the CE has a little influence on the potential distribution in the electrolyte at the back side of the WE. Therefore, an unprotected RE will give more stable potentials if it is moved from between the WE and CE to the back of the WE. The impedances of graphite anodes measured using a Li RE in this location are also shown in Fig. 2c and 3c. As expected, in both cells the effect of the reaction rates at the Li foil CEs had little influence on the impedances of the graphite WEs with this placement of the Li RE. The very small electrolyte resistance is due to the low electrical field behind the WE.

The influence of electrolyte field distribution on the unprotected Li RE potential.—When the cell is discharged (or charged) using GIT, the electric field and potential in the electrolyte changes and influences a Li RE (R_2) between the CE (C_2) and WE ($G_{1,2}$) to a greater extent than one on the other side (R_1). The potential difference between the two REs was directly measured during GIT measurement. Figure 4 shows the potential of the $G_{1,2}$ WE

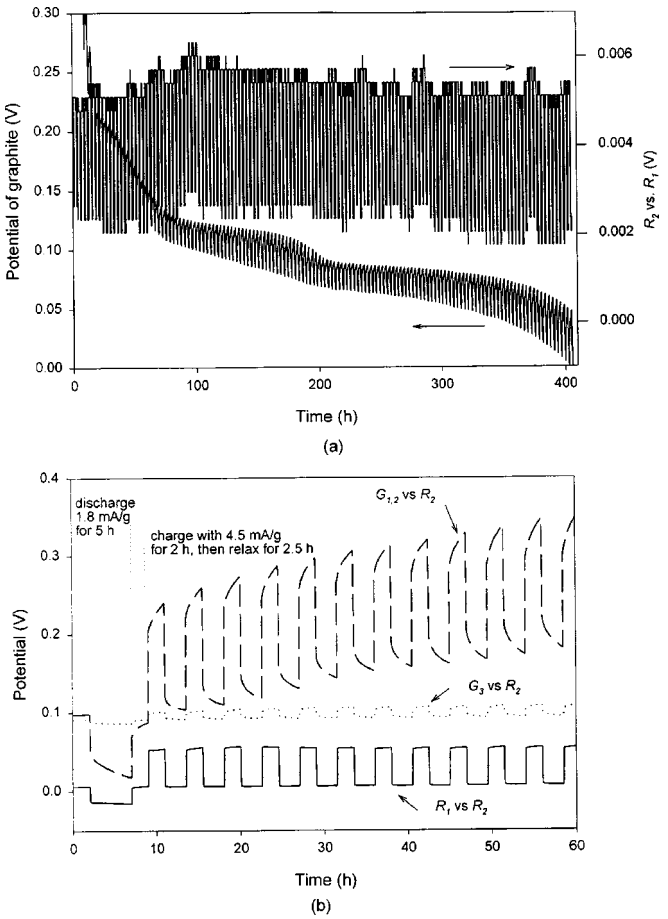

Figure 4. Potential of graphite WE ($G_{1,2}$), and voltage between R_1 and R_2 during $G_{1,2}$ GIT measurement using C_2(Li) as CE and R_2 as RE. (a) In cell C_2(Li)-R_2(Li)-$G_{1,2}$-R_1(Li)-C_1(Li) after one previous discharge/charge cycle. GIT discharge current profile, 3.0 mA/g for 1.0 h, followed by 2.0 h relaxation between each discharge. (b) In cell C_2(Li)-R_2(Li)-$G_{1,2}$-R_1(Li)-C_1(G_3) cells with GIT charge profile of 4.5 mA/g for 2.0 h followed by 2.5 h relaxation after GIT discharge to 0.02 V with 1.8 mA/g for 5.0 h followed by 2.5 h relaxation. Thirteenth cycle at 25°C, after cycling at 25°C for four cycles, −30°C for four cycles, and 65°C for four cycles. The potential of the G_3 CE (*vs.* R_2) also shown in Fig. 4b for comparison.

(*vs.* R_2) and voltage between RE_1 and RE_2 during GIT with C_2(Li) as counter and R_2 as reference electrodes in the C_2(Li)-R_2(Li)-$G_{1,2}$-R_1(Li)-C_1(Li) and C_2(Li)-R_2(Li)-$G_{1,2}$-R_1(Li)-C_1(G_3) cells. The C_2(Li)-R_2(Li)-$G_{1,2}$ half-cell in C_2(Li)-R_2(Li)-$G_{1,2}$-R_1(Li)-C_1(Li) cell configuration was discharged under GIT conditions at a current of 3.0 mA/g for 1.0 h, with 2.0 h at open circuit between each discharge after the first complete discharge-charge cycle at 25°C (Fig. 4a). GIT charging was applied in the C_2(Li)-R_2(Li)-$G_{1,2}$ half-cell in the C_2(Li)-R_2(Li)-$G_{1,2}$-R_1(Li)-C_1(G_3) cell configuration during the final cycle at 25°C at a current of 2.0 mA/g for 2.0 h, following 2.5 h relaxation. The reason for this was after cycling at different temperatures, the reaction kinetics of the $G_{1,2}$ WE were very slow, *i.e.*, high overpotentials were experienced. At open circuit, the R_2 potential was 2 mV higher than that of R_1 in the C_2(Li)-R_2(Li)-$G_{1,2}$-R_1(Li)-C_1(Li) cell. However, the voltage between R_2 and R_1 increased to around 5.0 mV when the $G_{1,2}$ WE was discharged using Li C_2, reverting back to 2 mV when the GIT discharge current was off (Fig. 4a). The voltage difference between R_1 and R_2 increased with overpotential of the $G_{1,2}$ WE but was

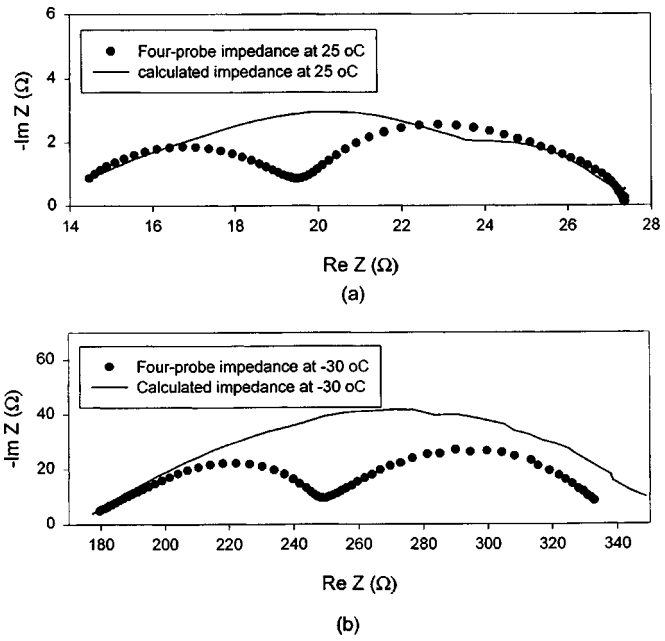

Figure 5. Impedances of electrolytes between REs R_1 and R_2 using four-probe measurement after 3rd discharge to 0.0 V at 25°C and after 6th discharge to 0.0 V at $-30°C$. Electrolyte impedances calculated from Eq. $Z_{ion} = Z_{G_3C_2} - Z_{G_3R_1G_{12}} - Z_{C_2R_2G_{12}}$ also shown in Fig. 4 to check validity of electrolyte impedance using four-probe method.

independent of its open-circuit potential (cf., Fig. 4a and b). The change in open circuit potential of the G_3 CE *vs.* R_2 was less than the R_1-R_2 voltage difference, because (*i*) the distance between G_3 and $G_{1,2}$ was two times greater than the distance between R_1 and $G_{1,2}$, and (*ii*) the reaction kinetics at G_3 were higher than those of R_1. This result suggests that the field change may also cause a slight change in the potential of R_1 in the reverse direction to that of R_2. Figure 4 gives direct evidence of the effect of electrolyte field perturbation on the local potential of an unprotected reference electrode.

Electronic and ionic conductivity measurements on graphite and TCO electrodes.—Since the local potential of the unprotected Li RE changes with changes in the field and potential distributions in the electrolyte, REs R_1 and R_2 may be used as sensors, and the Li ion conductivity of the porous graphite electrode can be measured using four-probe EIS measurement, *i.e.*, by connecting the Solatron interface terminals WE, RE_2, RE_1, and CE to the C_2, R_2, R_1, and G_3 electrodes, respectively (Fig. 1). Since the voltages were acquired from the two reference electrode RE_1 and RE_2 while a current was applied between the CE and WE, the EIS measured using this four-probe method are the Li-ion impedance of the electrolyte in the space between the two REs, *i.e.*, including the porous graphite electrode. Another method of obtaining the impedance of the electrolyte between the REs R_1 and R_2 in Fig. 1 is by subtraction of the impedances of the C_2 and G_3 electrodes from that of the C_2-G_3 cell, *i.e.*, $Z_{ion} = Z_{G_3C_2} - Z_{G_3R_1G_{12}} - Z_{C_2R_2G_{12}}$, which allows a check on both methods. Figure 5 shows the electrolyte impedance measured using the four-probe method after the second discharge to 0.0 V at 25°C and after the sixth discharge to 0.0 V at −30°C. The electrolyte impedances calculated from this equation are also shown in Fig. 5. Those measured impedance using the four-probe technique show two depressed semicircles, which may be attributed to the electrolyte impedance within the porous graphite electrode. The first semicircle in the high-frequency region may possibly represent the electrolyte impedance in the larger interparticle porosity, and the second in the low-frequency region may be due to the electrolyte impedance

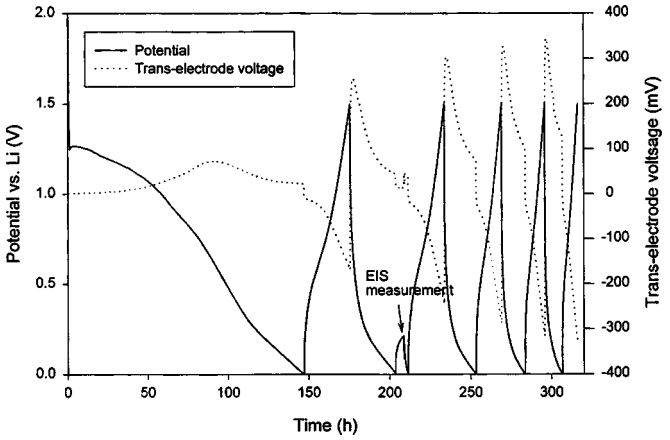

Figure 6. Potential and trans-electrode voltage during discharge-charge cycling at 5.4 mA/g current. EIS was performed following 5.0 h relaxation following the 2nd and 6th discharge to 0.0 V.

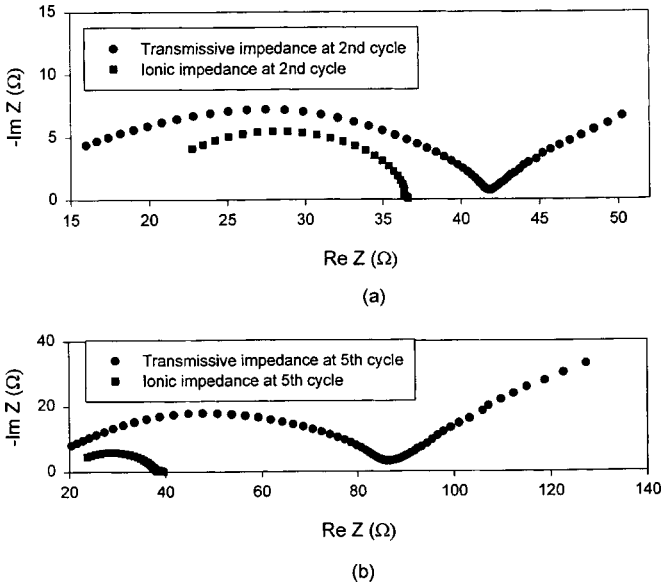

Figure 7. Transmissive and ionic impedances of $Sn_{1.3}Al_{0.3}Ti_{2.3}O_{1.95}(PO_4)_3$ measured after 5.0 h relaxation following the 2nd and 6th discharge to 0.0 V. The transmissive impedance was measured by connecting RE_2 and WE terminal of the Solatron interface together to T_1 side, and RE_1 plus CE to T_2 side. The ionic impedance was measured by using four-probe measurement.

in small channels between larger porous areas. Two depressed semicircles were also reported by Cho and Liu using the four-probe technique to measure the electrolyte impedance of glass-polymer composites.[6] The resistance determined from the intersection of the high-frequency line with the real axis in the complex impedance plot is the total electrolyte's resistance from the R_1 to G_1 side plus the electrolyte's resistance from the R_2 to G_2 side, *i.e.*, the electrolyte resistance outside of the graphite electrode. At −30°C, the diameter of the two depressed semicircles increased by a factor of 12.5 compared with the 25°C, which is the same as the increase in electrolyte resistance outside the graphite. This confirms that the two depressed semicircles of impedance result from the electrolyte's impedance within the porous graphite electrode. The impedance calculated by subtraction using the equation is very similar to that measured using the four-probe method, with the exception that only one depressed semicircle is present. This difference is possibly due to the accumulated error in the three impedances used in the calculation.

Electrodes consisting of a porous electronic conductor containing liquid electrolyte may be considered as mixed ionic-electronic conductor (MIEC), which can be modeled using an electrical transmission line, see Fig. 1, which shows that in each transmission line unit the electronic impedance is parallel with the ionic impedance. Previous results show that the transmissive impedance of porous graphite electrodes measured by connecting the RE_2 and WE terminals of the Solatron interface together to one side (G_1) of the WE and RE_1 plus CE to the other side (G_2) shows a pure electronic resistance (around 0.8 Ω) at 70 mV potential,[4] which remains at the same value at −30°C.[7] Hence, the transmissive impedance of a porous graphite electrode was largely attributed to ionic impedance, because the sum of the ionic impedances, including the electrolyte in the electrode, the SEI film, Li diffusion, and a portion of the charge-transfer impedance, are much higher than the electronic impedance. Thus, the use of methods for enhancing the ionic conductivity of porous graphite electrodes, *e.g.*, by decreasing electrode thickness and increasing percentage porosity, may increase their practical reaction kinetics.

Unlike graphite, the TCO electrode changes from the poor electronic conductor $Sn_{1.3}Al_{0.3}Ti_{1.7}O_{1.95}(PO_4)_3$ to the MIEC $Li_{1.3}Al_{0.3}Ti_{1.7}(PO_4)_3 + 1.95Li_2O + 1.3Sn$ during the first discharge process, and its electronic conductivity decreases with discharge-charge cycling due to the growth of Sn particles and pulverization. The decrease in electronic conductivity during discharge-charge cycles is demonstrated by the increase of trans-electrode voltage difference in Fig. 6. The decreases in electronic conductivity also result in high electrochemical polarization, giving a decreased capacity also shown in Fig. 6. To monitor the electronic and ionic conductivity, the transmissive and ionic impedances of TCO after the second and sixth discharge to 0.0 V were measured (Fig. 7). Unlike graphite electrodes, the ionic impedance of the TCO electrode shows one depressed semicircle. A possible reason for this is that the ionic impedance of $Li_{1.3}Al_{0.3}Ti_{1.7}(PO_4)_3$ matrix has overlapped the two depressed semicircles of the porous structure, forming a new depressed semicircle. The transmission impedance of TCO electrodes shows two depressed semicircles similar to those in the SnO_2 electrode. An arc in the low-frequency region (Fig. 7) is not seen because the final frequency used (10 mHz) was insufficiently low. For the graphite sandwich electrode, the resistance determined from the intersection of the low-frequency line with the real axis in the transmissive impedance plot is its electronic resistance. In Fig. 7, the electronic resistivity of the TCO electrode is much higher than ionic resistivity, and it rapidly increases over four discharge-charge cycles by at least a factor of two. During this interval, the electrolyte resistance within the porous electrode increases only slightly from around 17 to 20 Ω. Hence, the key to improving the cyclability of the TCO electrode is to enhance its electronic conductivity by decreasing particle pulverization on cycling and by inhibiting the growth of Sn particles.

Conclusions

The reliability of impedance and ionic conductivity of porous graphite and TCO WEs were investigated using five-electrode cells with two small Li foils as REs and two larger Li foils as CEs, or one Li foil and a graphite electrode identical to the WE. To obtain reliable impedance data for graphite anodes in three-electrode cells, the overall electrochemical reaction kinetic rate at the CE should be at least equal or greater than that of the WE. Moving the RE from a position between the WE and CE to behind the WE, or using two CEs at both sides of the WE can reduce the perturbation of the reference potential due to the local electric field. Both of these increase the reliability of WE impedance measurement. However, the use of two CEs or use of the RE behind the WE does not allow the determination of the correct electrolyte resistance between the RE and the WE from the impedance plot for the WE.

The ionic conductivity of porous electrodes in liquid electrolytes can be measured using the four-probe impedance method. Its reliability was checked by subtracting the impedances of two CEs from the impedance between the CEs. For porous graphite and $Sn_{1.3}Al_{0.3}Ti_{1.7}O_{1.95}(PO_4)_3$ electrodes prepared in this work, the limiting conductivity is ionic for graphite and electronic for $Sn_{1.3}Al_{0.3}Ti_{1.7}O_{1.95}(PO_4)_3$.

Texas A&M University assisted in meeting the publication costs of this article.

References

1. T. S. Ong and H. Yang, *Electrochem. Solid-State Lett.*, **4**, A89 (2001).
2. G. Hsieh, T. O. Mason, E. J. Garboczi, and L. R. Pederson, *Solid State Ionics*, **96**, 153 (1997).
3. J. Fu, *Solid State Ionics*, **96**, 195 (1997).
4. C. Wang, I. Kakwan, A. J. Appleby, and F. E. Little, *J. Electroanal. Chem.*, **489**, 55 (2000).
5. C. Wang, A. J. Appleby, and F. E. Little, *Electrochim. Acta*, **46**, 1793 (2001).
6. J. Cho and M. Liu, *Electrochim. Acta*, **42**, 1481 (1997).
7. C. Wang, A. J. Appleby, and F. E. Little, *J. Electrochem. Soc.*, **149**, A754 (2002).